Time-dependent density-functional study of the alignment-dependent ionization of acetylene and ethylene by strong laser pulses

Arthur Russakoff,[1] Sergiy Bubin,[2] Xinhua Xie,[3] Sonia Erattupuzha,[3] Markus Kitzler,[3] and Kálmán Varga[1]

[1]*Department of Physics and Astronomy, Vanderbilt University, Nashville, Tennessee 37235, USA*

[2]*Department of Physics, School of Science and Technology, Nazarbayev University, Astana 010000, Kazakhstan*

[3]*Photonics Institute, Vienna University of Technology, A-1040 Vienna, Austria, EU*

(Received 17 November 2014; published 19 February 2015)

The alignment-dependent ionization of acetylene and ethylene in short laser pulses is investigated in the framework of the time-dependent density-functional theory coupled with Ehrenfest dynamics. The molecular alignment is found to have a substantial effect on the total ionization. Bond stretching is shown to cause an increase of the ionization efficiency, i.e., enhanced ionization, in qualitative agreement with previous theoretical investigations. It is also demonstrated that the enhanced ionization mechanism greatly enhances the ionization from the inner valence orbitals, and the ionization of the inner orbitals is primarily due to their extended weakly bound density tails.

DOI: 10.1103/PhysRevA.91.023422 PACS number(s): 33.80.Rv, 79.77.+g, 82.53.−k

I. INTRODUCTION

The ionization of molecules with intense laser pulses is a complex process due to the interplay of the time-varying external potential introduced by the strong laser electric field and the Coulomb interaction between the electrons [1–6]. The final and seemingly close aim is not only understanding but also controlling the ionization dynamics to influence chemical reactions at the femtosecond time scale [7–10]. The interaction of molecules with laser fields obviously depends on the laser parameters such as field strength, frequency, pulse shape, and carrier envelope phase. It also depends on the directionality of the molecular frame relative to the laser field's polarization axis, which will hereafter be referred to simply as the alignment. Over the last decade experimental investigation of photoelectron angular distributions from aligned molecules has become possible [11–15]. This allows a clear comparison between experiment and theory without the obscuring effect of averaging over alignments [16]. Experiments also reveal a difference in the ionization from different molecular orbitals reflecting the nodal symmetry of the molecular wave functions [17–26]. Beyond mere structural effects it is also found that the total ionization yield can be increased by a coherent amplification of lower orbitals [19]. Finally, one of the most important mechanisms in molecular ionization is enhanced ionization [27–29], where highly efficient ionization occurs at critical nuclear separations. Recently, experimental evidence has been found that this process may also take place at many bonds in parallel in a polyatomic molecule [30,31].

In this paper the time-dependent density-Functional theory (TDDFT) [32] coupled with the Ehrenfest dynamics [33] will be used to study the alignment dependence of ionization in short laser pulses. Two small molecules, acetylene and ethylene, exposed to laser pulses of various intensity and durations will be used to analyze how the time-dependent Kohn-Sham orbitals' ionization dynamics couple with the ions' dynamics. We will study (i) the enhanced ionization in a restricted fixed-ion model as well as in a fully dynamical simulation, (ii) the alignment dependence of the ionization, and (iii) the role of the molecular orbitals and their different symmetries in the ionization and fragmentation dynamics.

From a numerical point of view these are difficult problems because the solution of the time-dependent Schrödinger equation is very complicated beyond simple one- or two-electron systems. Pioneering works aiming to set up a simple framework to understand ionization include the model where the electrons and nuclei are treated classically [29] and the single-active-electron model [34], originally formulated for atoms, which assumes that the ionization of atoms can be described by an appropriately modified hydrogenlike model. This model was later extended for molecules [35] and has been used to study the ionization of diatomic molecules [36,37].

Another theoretical approach, the time-dependent Hartree-Fock (TDHF) [38–40] method, was also used to study the physical mechanisms behind the fragmentation of molecules in intense laser fields. These works have focused on the total and orbital ionization efficiencies and the enhanced ionization mechanism of acetylene (C_2H_2) by exploring the electron dynamics.

Enhanced ionization is described as a three-step process [29]. First, the C-H bonds expand to a critical separation R_c. Then, the increased C-H bond length leads to highly efficient ionization of the molecule [30,31]. After the enhanced ionization, the molecule often undergoes fragmentation, ejecting the hydrogen ions. With the TDHF approach, it was shown that as the C-H bond lengths are symmetrically increased, the ionization efficiency of each orbital also increases until the bond lengths reach a critical separation after which the ionization efficiency plateaus, thus demonstrating the enhanced ionization mechanism. The TDHF approach is expected to capture the essence of the laser-induced electron dynamics. However, in these simulations the ion positions were fixed for the duration of the laser pulse.

A dynamically more complete picture of the electron-nuclear dynamics and ionization can be given in the framework of TDDFT. TDDFT has been used to study the Coulomb explosion of deuterium [41,42], biomolecules immersed in liquid water [43], water clusters [44], and small hydrocarbon molecules [16]. TDDFT simulations have also been used to describe the electron-ion dynamics of H_2S [45] and to simulate the Coulomb imaging of biphenyl [46].

The plan of this paper is as follows. After this introduction we briefly describe the computational approach in Sec. II. Section III presents the results and analysis of the ionization mechanisms of the acetylene and ethylene molecules for different alignments and laser fields. The paper is closed with a summary in Sec. IV.

II. COMPUTATIONAL METHOD

The electron dynamics of the simulation were modeled using TDDFT on a real-space grid with real-time propagation. Core electrons, which are difficult to handle computationally, were represented using norm-conserving Troullier-Martins pseudopotentials [47].

In the first stage of the calculation the initial (ground) state of the system is prepared by performing the ground-state DFT calculation. Next, the time-dependent Kohn-Sham orbitals ψ_k are determined by solving the time-dependent Kohn-Sham equation,

$$i\hbar\frac{\partial\psi_k(\mathbf{r},t)}{\partial t} = H\psi_k(\mathbf{r},t), \tag{1}$$

where k is a quantum number labeling the orbital. The (Kohn-Sham) Hamiltonian is given by

$$H = -\frac{\hbar^2}{2m}\nabla^2_{\mathbf{r}} + V_{\mathrm{H}}[\rho](\mathbf{r},t) + V_{\mathrm{XC}}[\rho](\mathbf{r},t) + V_{\mathrm{ext}}(\mathbf{r},t). \tag{2}$$

Here ρ denotes the electron (number) density, which is defined by a sum over all occupied orbitals:

$$\rho(\mathbf{r},t) = \sum_{k=1}^{\infty} f_k|\psi_k(\mathbf{r},t)|^2, \tag{3}$$

where f_k is the occupation number of the orbital ψ_k. f_k may take on the values 0, 1, and 2 ($f_k = 2$ is permitted via spin degeneracy). f_k is subject to the constraint $\sum_{k=1}^{\infty} f_k = N$, where N is the total number of (valence) electrons in the system.

V_{H} in Eq. (2) is the Hartree potential, defined by

$$V_{\mathrm{H}}(\mathbf{r},t) = \int d\mathbf{r}'\frac{\rho(\mathbf{r}',t)}{|\mathbf{r}-\mathbf{r}'|}, \tag{4}$$

and it accounts for the electrostatic Coulomb interactions between electrons.

V_{XC} is the exchange-correlation potential, whose exact form is a complicated functional of the entire history of the electron density. It will be approximated using the adiabatic local-density approximation (ALDA) with the parametrization of Perdew and Zunger [48].

The last term in Eq. (2), V_{ext}, is the external potential, which includes the implicitly time-dependent potential due to the ions V_{ion} and the explicitly time-dependent potential due to the electric field of the laser V_{laser}. V_{ion} is a sum of norm-conserving pseudopotentials by Troullier and Martins [47] centered at each ion.

V_{laser} is described using the dipole approximation, $V_{\mathrm{laser}} = \mathbf{r}\cdot\mathbf{E}(t)$, with the time-dependent electric field given by

$$\mathbf{E}(t) = \hat{\mathbf{k}}E_{\max}\exp\left[-\frac{(t-t_0)^2}{2a^2}\right]\sin(\omega t). \tag{5}$$

The parameters a, t_0, and $E_{\max}$ define the width, the initial position of the center, and the maximum amplitude of the Gaussian envelope, respectively. ω describes the frequency of the laser, and $\hat{\mathbf{k}}$ is a unit vector defining the polarization of the electric field.

The time-dependent orbitals, from which the electron (number) density is calculated, may be formally time propagated from the initial state to some time t by using the time-evolution operator,

$$U(0,t) = \mathcal{T}\exp\left[-\frac{i}{\hbar}\int_0^t H(\mathbf{r},t')dt'\right], \tag{6}$$

where $\mathcal{T}$ denotes time ordering. In practice, $U(t,0)$ is split into a product of multiple time-evolution operators, each corresponding to a short time step δt,

$$U(0,t) = \prod_q U(t_q,t_q+\delta t), \quad t_q = q\delta t. \tag{7}$$

In our calculations, $U(t_q,t_q+\delta t)$ is approximated using a fourth-order Taylor expansion, so that the propagation of the Kohn-Sham orbitals over a very short time step δt is given by

$$\psi_k(\mathbf{r},t_q+\delta t) \approx \sum_{n=0}^{4}\frac{1}{n!}\left(-\frac{i\delta t}{\hbar}H(\mathbf{r},t_q)\right)^n\psi_k(\mathbf{r},t_q). \tag{8}$$

The Taylor propagation, although not unconditionally stable, gives a very stable propagation provided that the time step is chosen to be suitably small. The advantage of the Taylor propagation is that it is very simple as it only requires the repeated action of the Hamiltonian on the wave function. A review and comparison of the advantages and disadvantages of different time-propagating schemes in TDDFT can be found in Ref. [49].

In real-space TDDFT the Kohn-Sham orbitals are represented at discrete points in real space. In practice these discrete points are organized in a uniform rectangular grid. The accuracy of numerical calculations is controlled by adjusting the grid spacing. At the walls of the simulation cell boundary conditions must be enforced. Typically, the wave functions are set to zero at the walls. However, this zero-boundary condition can lead to an unphysical reflection of the wave function off the walls of the simulation cell. To prevent this from happening we implemented a complex absorbing potential (CAP). This potential is nonzero only in the region of space close to the walls. The functional form of the CAP used in our simulations is taken from Manolopoulos [50]. This negative, imaginary CAP is derived from a physically motivated differential equation, and its form is

$$-iw(x) = -i\frac{\hbar^2}{2m}\left(\frac{2\pi}{\Delta x}\right)^2 f(y), \tag{9}$$

where x_1 is the start and x_2 is the end of the absorbing region, $\Delta x = x_2 - x_1$, $c = 2.62$ is a numerical constant, m is the electron's mass, and

$$f(y) = \frac{4}{c^2}\left(\frac{1}{(1+y)^2} + \frac{1}{(1-y)^2} - 2\right),$$
$$y = \frac{(x-x_1)}{\Delta x}. \tag{10}$$

As the molecule is ionized by the laser field, electron density will travel to the edge of the simulation box, where it is absorbed by the CAP. The integral of the electron density over the volume of the box,

$$N(t) = \int_V \rho(\mathbf{r},t) d^3x, \tag{11}$$

will therefore diverge from the initial electron number $N(0)$. Since, in general, $N(t)$ is not an integer, we will refer to it henceforth as the fractional electron number. We interpret $N(0) - N(t)$ as the total ionization of the molecule.

Motion of the ions in the simulations is treated classically based on the Ehrenfest theorem [33]. The quantum forces on the ions, which are due to the electrons, are given by the derivatives of the expectation value of the total electronic energy with respect to the ionic positions. These forces are then fed into Newton's second law, giving

$$M_i \frac{d^2\mathbf{R}_i}{dt^2} = Z_i \mathbf{E}_{\text{laser}}(t) + \sum_{j\neq i}^{N_{\text{ions}}} \frac{Z_i Z_j (\mathbf{R}_i - \mathbf{R}_j)}{|\mathbf{R}_i - \mathbf{R}_j|^3} - \nabla_{\mathbf{R}_i} \int V_{\text{ion}}(\mathbf{r},\mathbf{R}_i)\rho(\mathbf{r},t) d\mathbf{r}, \tag{12}$$

where M_i and Z_i are the mass and pseudocharge (valence) of the ith ion, respectively, and N_{ions} is the total number of ions.

The computational results presented in the next section have been calculated by using the following parameters. The $L_x \times L_y \times L_z$ box size is $L_x = 40$ Å, $L_y = L_z = 34$ Å for C_2H_4 and $L_x = L_y = L_z = 34$ Å for C_2H_2. The C-C bond lies in the x direction. The grid spacing is 0.25 Å in each direction. The CAP starts 5 Å from the boundary. The time step for the propagation of the wave function is $\delta t = 0.0007$ fs. The equation of the ionic motion [Eq. (12)] is solved with the Verlet algorithm with a time step of 0.0028 fs. These parameters lead to very well converged results. The calculated ionization potential is 11.0 eV for C_2H_4 and 11.8 eV for C_2H_2 (the experimental values are 10.5 eV for C_2H_4 and 11.4 eV for C_2H_2 [51]).

III. RESULTS AND ANALYSIS

Using the time-dependent density-functional theory [32] and Ehrenfest dynamics [33], we have studied the ionization mechanism of acetylene and ethylene exposed to laser pulses carried at a wavelength of 800 nm with various peak intensities and durations. Our choice of the two molecules is motivated, on the one hand, by previous experimental [30,31] and theoretical [38–40] studies on these molecules and, on the other hand, by the different complexities and structures of them. The acetylene molecule is one step from the diatomic molecules towards more complicated structures. It is still a linear molecule, so the relative direction of the laser field and the molecular frame is given by a single angle, but it has two nonequivalent bonds: the strong threefold C-C bond in the middle and the two C-H bonds at the ends. Ethylene is one step further towards the larger hydrocarbon molecules. It has a coplanar geometry with a H-C-H angle close to the ideal 120° for sp^2 hybridized carbon. We will study the ionization from different orbitals, the dependence of ionization on the alignment of the molecule, and the ionization from bond-stretched configurations. The goal of this study is to understand the enhanced ionization mechanism beyond the static TDHF picture and to investigate the role of the molecular alignment in the ionization process.

A. C_2H_2

The ionization and molecular dynamics of acetylene, C_2H_2, have been studied by varying the intensity and duration of the laser field for parallel and perpendicular alignments of the molecule relative to the laser polarization direction. We have studied the response to nine different laser fields (see Table I) with intensities and pulse durations typical in experiments [31].

1. Acetylene in a laser field polarized parallel to the molecular axis

Before turning to the detailed results of the TDDFT simulations we show a simple picture that captures the essence of the electron-nuclear dynamics in acetylene aligned parallel to the laser field polarization direction. In this picture we investigate the separate actions of the different potentials, i.e., Hartree potential [Eq. (4)], the local part of the exchange correlation potential, the ionic potential, and the external potential of the laser field. Figure 1 shows snapshots at different times during and after the laser pulse of the total potential, i.e., the sum of all the potentials, and the electron density along the x axis, to which both the molecule and laser field polarization are parallel.

The total potential shows two shallow and two deep wells corresponding to the positions of the hydrogen and carbon nuclei. The acetylene molecule is subject to a few-cycle laser pulse with a duration of 4.5 fs and a laser peak of 14×10^{14} W/cm^2. Here and throughout the paper, the pulse duration is defined as the FWHM of intensity. In the second snapshot [Fig. 1(b)], the potential declines, and the tail of the density spreads out to the right. Next, in Fig. 1(c), the laser field changes direction, the potential inclines, and the density tail spreads out more towards the left side. At this time (15.75 fs) the laser has reached its peak amplitude, and the hydrogen nuclei are already moving outward, although the distance from the original position is only 0.3 Å. The next snapshot [Fig. 1(d)] illustrates the situation at the next peak of the laser. In these snapshots one can also compare the laser potential to the potential of the atomic cores, and one sees that the ionization is more probable from and around the shallow hydrogen nuclei. The snapshots also show the ionization by the visible decrease of the total density. The number of valence electrons drops from 10 to 6 by the end of the laser pulse [see Fig. 3(a)]. The last two snapshots depict the potential and the density after the laser pulse, showing the motion of the emitted protons.

The motion of the nuclei and the eventual fragmentation is caused by the interplay of the forces arising from the electron localization caused by the laser and the direct force that the laser imposes on the charged nuclei. The latter force is given by the first term on the right-hand side of Eq. (12). The resulting forces on the H^+ ions are illustrated in Fig. 2(a). Consider the peak of the laser field at 15.75 fs. The laser field's polarization points to the right, and it applies a rightward force on the

TABLE I. Orbital ionization dynamics of C_2H_2 and C_2H_4 for various laser pulses and molecular alignments. The first column gives the kinetic energy (KE) of the hydrogen ions (per ion). The subsequent columns show the occupation number of each Kohn-Sham orbital and the total electron number at the end of the simulation. C_2H_2 has only five occupied orbitals (HOMO, HOMO-1, HOMO-2, HOMO-3, and HOMO-4), and hence, the column for the occupation of HOMO-5 has been marked with an X to indicate that it is not applicable in this case.

	KE (eV)	HOMO	HOMO-1	HOMO-2	HOMO-3	HOMO-4	HOMO-5	Number of electrons
C_2H_2, parallel								
4×10^{14} W/cm^2, 4.5 fs	0	1.7	1.7	1.9	1.9	2.0	X	9.1
7×10^{14} W/cm^2, 4.5 fs	0	1.5	1.5	1.7	1.7	2.0	X	8.3
14×10^{14} W/cm^2, 4.5 fs	11.7	1.2	1.2	1.1	1.2	1.9	X	6.6
4×10^{14} W/cm^2, 15 fs	0	1.5	1.5	1.8	1.6	2.0	X	8.5
7×10^{14} W/cm^2, 15 fs	14.9	1.3	1.3	0.3	0.5	1.9	X	5.3
14×10^{14} W/cm^2, 15 fs	22.8	1.1	1.1	0.6	0.2	1.6	X	4.6
4×10^{14} W/cm^2, 25 fs	0	1.5	1.5	1.7	1.5	2.0	X	8.1
7×10^{14} W/cm^2, 25 fs	16.5	1.3	1.3	0.7	0.2	1.9	X	5.4
14×10^{14} W/cm^2, 25 fs	22.5	0.9	0.9	0.5	0.1	1.4	X	3.6
C_2H_2, 22.5°								
4×10^{14} W/cm^2, 4.5 fs	0	1.7	1.5	1.9	1.9	2.0	X	9.0
7×10^{14} W/cm^2, 4.5 fs	0	1.6	1.3	1.8	1.8	2.0	X	8.4
14×10^{14} W/cm^2, 4.5 fs	8.5	1.3	1.0	1.4	1.4	1.9	X	7.0
C_2H_2, 45°								
4×10^{14} W/cm^2, 4.5 fs	0	1.8	1.3	2.0	2.0	2.0	X	9.0
7×10^{14} W/cm^2, 4.5 fs	0	1.7	1.0	1.9	1.9	2.0	X	8.4
14×10^{14} W/cm^2, 4.5 fs	4.9	1.5	0.7	1.7	1.5	2.0	X	7.3
C_2H_2, perpendicular								
4×10^{14} W/cm^2, 4.5 fs	0	1.9	1.1	2.0	2.0	2.0	X	9.0
7×10^{14} W/cm^2, 4.5 fs	0	1.8	0.8	1.9	2.0	2.0	X	8.5
14×10^{14} W/cm^2, 4.5 fs	0	1.6	0.4	1.7	1.9	2.0	X	7.6
4×10^{14} W/cm^2, 15 fs	0	1.9	0.7	2.0	2.0	2.0	X	8.6
7×10^{14} W/cm^2, 15 fs	0	1.7	0.3	1.9	2.0	2.0	X	8.0
14×10^{14} W/cm^2, 15 fs	10.0	1.4	0.0	0.9	1.9	2.0	X	6.3
4×10^{14} W/cm^2, 25 fs	0	1.9	0.6	2.0	2.0	2.0	X	8.4
7×10^{14} W/cm^2, 25 fs	0	1.7	0.2	1.9	2.0	2.0	X	7.8
14×10^{14} W/cm^2, 25 fs	13.7	1.4	0.0	0.4	1.9	2.0	X	5.7
C_2H_4, C-C parallel								
8×10^{14} W/cm^2, 9 fs	5.9	1.3	1.0	1.3	1.3	1.6	2.0	8.5
8×10^{14} W/cm^2, 17 fs	18.8	1.2	0.4	0.4	0.3	1.1	1.8	5.1
C_2H_4, C-C perpendicular								
8×10^{14} W/cm^2, 9 fs	0.2	1.6	0.6	1.5	1.6	1.9	2.0	9.2
8×10^{14} W/cm^2, 17 fs	9.6	1.5	0.1	0.6	1.0	1.5	2.0	6.8
C_2H_4, perpendicular								
8×10^{14} W/cm^2, 9 fs	0	0.2	2.0	1.7	2.0	2.0	2.0	9.8
8×10^{14} W/cm^2, 17 fs	0	0.0	2.0	1.7	2.0	2.0	2.0	9.6

two hydrogen ions. However, the laser also causes the fast moving electrons to move to the left, as shown in Fig. 2(b). For the left hydrogen ion, the excess of electrons will induce additional Coulomb shielding between the H^+ and the other ions, which manifests as a leftward force. This force cancels with the laser force, and the total force is nearly zero. For the right hydrogen atom, the reduction of electrons reduces the Coulomb shielding, which manifests itself as a rightward force. This force will be additive with the laser force. Hence, the total force is much greater than the laser force alone. This picture is reversed when the electric field's polarization is reversed.

We have also compared the force acting on the protons to a model force [29], which is calculated as the sum of the direct laser force and the Coulomb force between a proton and a triply charged C_2H fragment. This quantity over time is depicted in Fig. 2(c). In the model force calculation the trajectory of the TDDFT simulation is used for the position of the particles, and one electron is removed from each atom, corresponding to the ionization of roughly four electrons, shown in Fig. 2(b). As shown in Fig. 2(c), the sudden ionization leads to the removal of four electrons right after the peak of the laser field (around 17 fs), and after that time the model and TDDFT force are similar. The Coulomb dissociation starts at around the peak of the laser field, and at 17 fs the protons have moved about 2 Å. Hence, the bond is definitely broken, and the simple Coulomb model captures the dynamics.

Now we turn to a more detailed analysis of the ionization mechanism using the full TDDFT model and allowing the

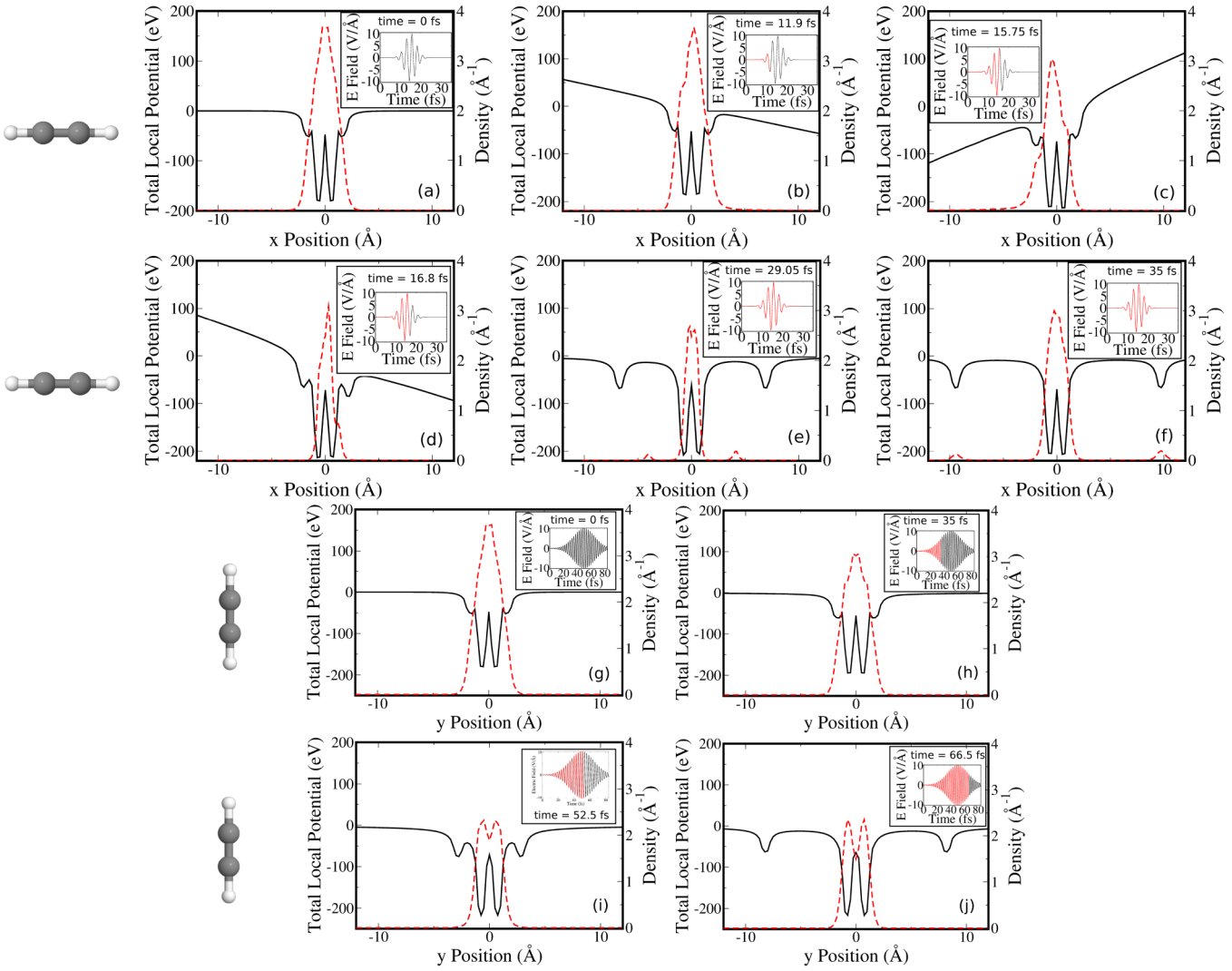

FIG. 1. (Color online) (a)–(f) Selected snapshots of the total local potential (solid black line) and the density (dashed red line) for C_2H_2 along the alignment axis of the molecule (x axis), integrated out to 2 Å perpendicular to the x axis. The laser peak intensity is 14×10^{14} W/cm^2, and the pulse duration is 4.5 fs. The total local potential consists of the Hartree potential, the local part of the exchange correlation potential, the ionic pseudopotential, and the external potential of the laser field. The insets show the simulation time and the laser pulse highlighted up to the current simulation time. (a) shows the unperturbed initial state. In (b) the density spreads towards one end of the simulation box due to the external potential. In (c) the electric field has switched direction, and the density spreads towards the opposite end of the simulation box. In (d), the electric field has switched direction again. In (e) and (f) the hydrogen atoms have been split off and are ejected towards the ends of the simulation box. (g)–(j) Selected snapshots of the total local potential (solid black line) and the density (dashed red line) along the alignment axis of C_2H_2 (y), integrated out to 2 Å perpendicular to the y axis. The laser polarization direction is x, the peak intensity is 14×10^{14} W/cm^2, and the pulse duration is 25 fs. (g) shows the unperturbed initial state. In (h) the density has decreased as the laser ionizes the molecule. In (i) the density has further decreased, and the hydrogen ions have begun to dissociate from the molecule. In (j) the hydrogen ions have dissociated and are ejected towards the ends of the simulation box.

ions to move according to the Ehrenfest dynamics. Before we begin this discussion we note that due to the Ehrenfest scheme each simulation represents only an averaging over all possible nuclear fragmentation channels. At low intensity and pulse width the probability of fragmentation is small, and the dissociation of the C-H bonds does not occur in our simulations. A Coulomb explosion is observed for higher intensities and longer pulses (see Table I).

We first consider the case of 4.5-fs laser pulses with three different peak intensities. The total ionization is plotted in Fig. 3. As expected, the number of electrons removed increases with the intensity of the laser. After the ionization exceeds a critical electron number the molecule undergoes a Coulomb explosion.

Figure 4 shows the ground-state Kohn-Sham orbitals of acetylene and snapshots of the orbitals at the peak of the laser field. The highest occupied molecular orbital (HOMO) and HOMO-1 are energy degenerate, and their shapes are exactly 90° rotations of one another. HOMO-2, HOMO-3, and HOMO-4 are all cylindrically symmetric, but each has its own nodal symmetry. Due to their different symmetries, the orbitals each ionize with a different angular distribution

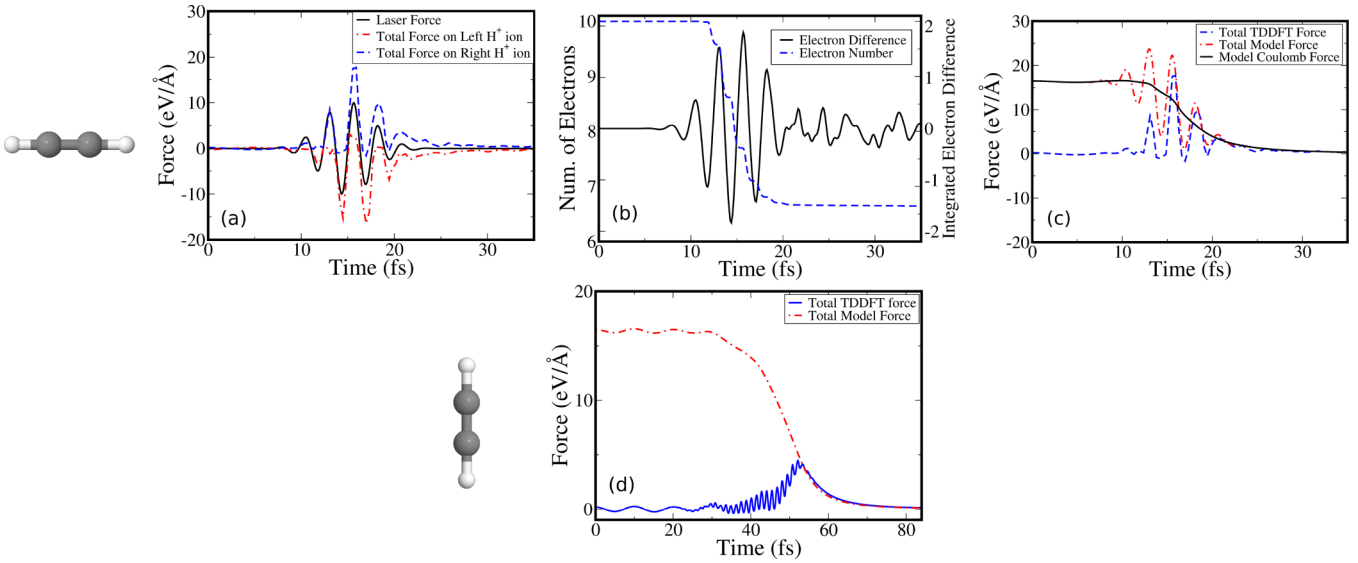

FIG. 2. (Color online) (a)–(c) Acetylene in a laser field with a polarization direction parallel to the molecular axis, an intensity of 14×10^{14} W/cm^2, and a pulse duration of 4.5 fs. (a) The total force on the two hydrogen ions, which is the sum of the laser force, the ion-ion forces, and the electron-ion force. The laser force (black line) is equal for both hydrogen ions. (b) Fractional electron number, $\int \rho d^3x$, and the difference between the fractional electron numbers in the left side of the box and the right side of the box, $\int_{x<0} \rho\ d^3x - \int_{x>0} \rho\ d^3x$. (c) The Coulomb force and total force on the right hydrogen ion calculated assuming a simple model where each atom loses one electron instantaneously. The ion-ion distances used in this simple force calculation are taken from the TDDFT simulation. The total force from the TDDFT simulation is shown for comparison. (d) The total force along the y (molecular) axis on a hydrogen ion calculated by TDDFT for a laser field polarized along x (perpendicular alignment) and a pulse peak intensity of 14×10^{14} W/cm^2 and pulse duration of 25 fs. A simple model calculation for the Coulomb force on a hydrogen ion is also shown, with the same details as in (c). The ion moves essentially along the y (molecular) axis for the duration of the simulation with only a small oscillation (<0.02 Å) along the x (polarization) axis.

(right column of Fig. 4). Despite the orbitals' different nodal symmetries, single-particle energies, and angular distributions, the total ionization is very similar for HOMO, HOMO-1, HOMO-2, and HOMO-3 [see Fig. 3(a)]. The HOMO-4 orbital is significantly more deeply bound, and the ionization is small. The ionizations from the HOMO and HOMO-1 orbitals are nearly identical due to their energy degeneracy and similar symmetry. At low intensity, HOMO and HOMO-1 are the most ionized. As the intensity of the laser is increased, the inner orbitals, HOMO-2 and HOMO-3, are increasingly ionized. The most significant change is that in the strongest field the HOMO-2 orbital has the largest ionization. This is due partly to its complicated nodal structure and partly to the fact that the time-dependent Kohn-Sham binding energy (not shown) of this orbital decreases the most in the laser field.

According to the enhanced ionization model, as the C-H bond length of the molecule increases, there is a corresponding increase in the ionization rate. To check this Ref. [40] studied the ionization from bond-stretched molecular states using the TDHF approach. This model is an approximation since the laser pulse increases the bond length and ionizes the molecule simultaneously. Hence, in the stretched configurations the electron number is decreased, and these configurations are positively charged. For simplicity this effect was neglected. While our TDDFT simulations with the Ehrenfest dynamics do not suffer from this drawback, it is unclear how important the enhanced ionization effect is to the total ionization. We have therefore repeated the TDDFT calculations without Ehrenfest dynamics, i.e., with ions held fixed in the ground-state geometry or in bond-stretched geometries.

Figure 3(a) shows that for low fields the total ionization for moving nuclei and for nuclei fixed in the ground state geometry is nearly the same. This is not surprising as the ions barely move in the low fields. At 14×10^{14} W/cm^2, the two C-H bond lengths increase (asymmetrically) from 1.076 to 3.744 Å and to 3.909 Å by the time the ionization completes. The bond stretching causes an additional ionization of 0.9 electron relative to the fixed-ion case. This additional ionization comes primarily from the increased ionization of the inner orbitals, HOMO-2 and HOMO-3. When the ion positions are fixed in the ground-state geometry ($R_{\mathrm{C-H}} = 1.076$ Å), the ionization of the inner orbitals is suppressed [see Fig. 3(i)].

To further investigate the effect of bond stretching on the ionization, we have repeated the fixed-ion calculations for several extended geometries. Figure 3(i) shows that the total ionization increases with the C-H bond lengths, in qualitative agreement with Lötstedt *et al.* [40]. If the ions are fixed in the ground-state geometry, HOMO and HOMO-1 are ionized the most. As the C-H bond length is increased, HOMO-2 and HOMO-3 become more ionized. At a C-H bond length of $R = 1.8$ Å the ionization is dominated by the inner orbitals, HOMO-2 and HOMO-3. At the same time the ionization of HOMO and HOMO-1 is slightly suppressed. The increased ionization of HOMO-2 and HOMO-3 is partially because they are less tightly bound in the stretched configurations [see Fig. 5(a)]. The fixed-ion model qualitatively matches the orbital dynamics seen with the Ehrenfest dynamics [Fig. 3(a)],

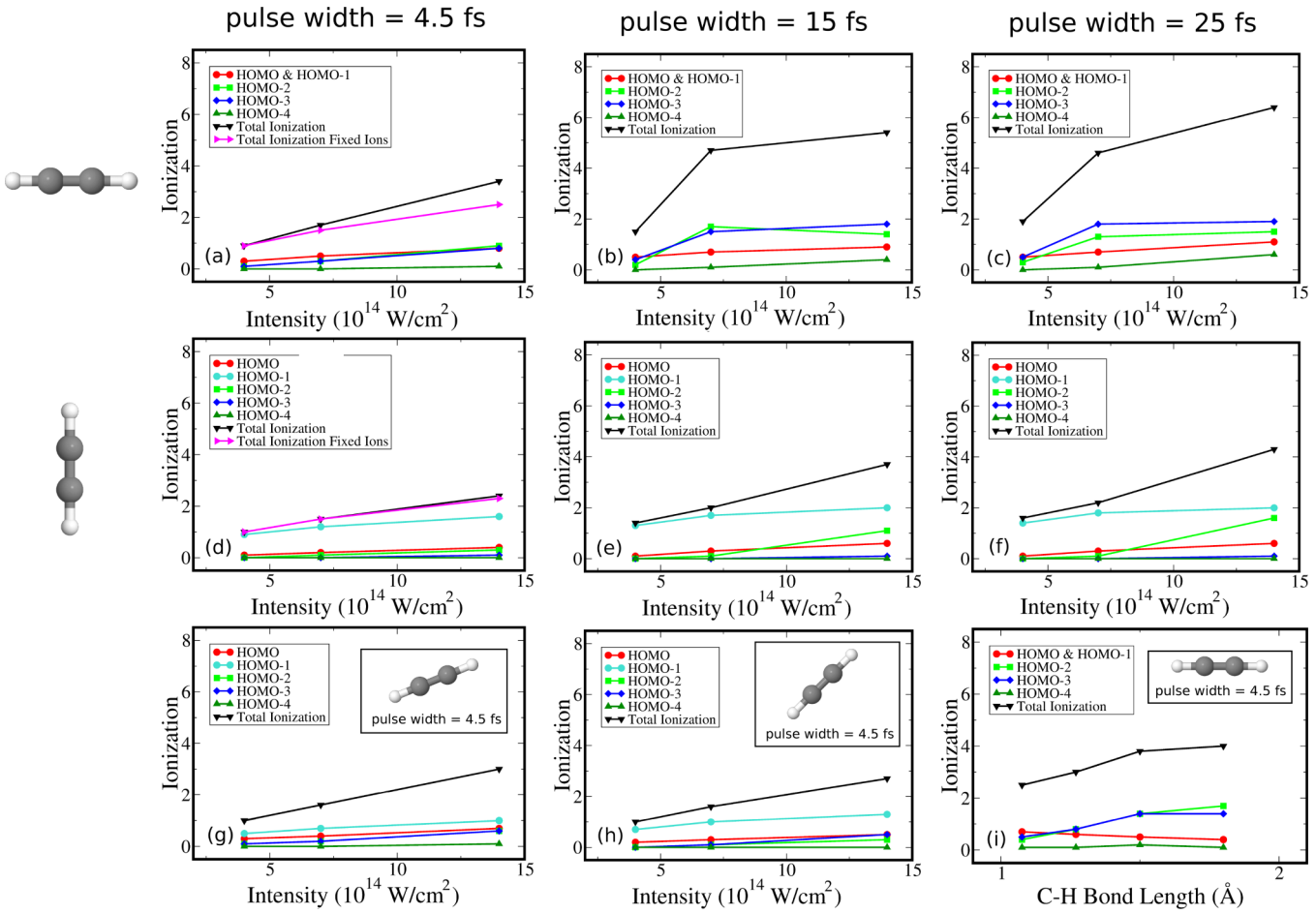

FIG. 3. (Color online) (a)–(f) Total and orbital ionization as a function of laser intensity for C_2H_2 for a pulse duration of (a), (d) 4.5 fs, (b), (e) 15 fs, and (c), (f) 25 fs for alignments of the molecule (a)–(c) parallel and (d)–(f) perpendicular to the laser polarization direction. Additionally, in (a) and (d) the total ionization for fixed ions is shown. (g) and (h) Total and orbital ionization as a function of laser intensity for angles of 22.5° and 45° between the molecular axis and laser polarization direction, respectively. The laser pulse duration is 4.5 fs. (i) Ionization as a function of C-H bond length for a laser peak intensity of 14×10^{14} W/cm^2 and a pulse duration of 4.5 fs.

where the ionization of HOMO-2 and HOMO-3 overtakes HOMO and HOMO-1 at intensities high enough to cause bond stretching. Hence, the enhanced ionization mechanism works primarily by ionizing the inner orbitals.

Finally, we have run calculations with longer pulses to see if a Coulomb explosion appears within the Ehrenfest scheme at lower intensities. Table I shows a summary of results for 15- and 25-fs pulses over three intensities. The longer pulses increase the ionization, and the Coulomb explosion appears at an intensity of 7×10^{14} W/cm^2. At 4×10^{14} W/cm^2 the probability of bond breaking remains too low for a Coulomb explosion to appear in the simulations. At 14×10^{14} W/cm^2 the carbon ions also dissociate. The kinetic energy of the emitted protons is two times larger for the 15-fs pulse than for the 4.5-fs pulse (see Table I), but a further increase of the pulse duration does not increase the kinetic energy in this case.

Figures 3(b) and 3(c) show the orbital and total ionization versus intensity for pulse durations 15 and 25 fs. At 4×10^{14} W/cm^2, where bond stretching does not occur, HOMO and HOMO-1 remain the most ionized orbitals. At the higher intensities the enhanced ionization due to bond stretching greatly increases the ionization of HOMO-2 and HOMO-3. Once again, the ionization of the inner orbitals surpasses that of HOMO and HOMO-1, and now the effect is much more pronounced.

Figures 3(a)–3(c) show that in our simulations HOMO-2 and HOMO-3 dominate the ionization in high-intensity laser fields with long pulse widths. As we have noted previously, HOMO-2 and HOMO-3 are less deeply bound in stretched configurations [see Fig. 5(a)], and this explains why HOMO-2 and HOMO-3's ionization increases dramatically with stronger pulses. However, we have not explained why HOMO-2 and HOMO-3's ionization surpasses that of HOMO and HOMO-1. Several recent experiments [18,19,53–59] have also observed greater ionization from the inner orbitals. The experiments attribute this finding to (i) the different geometries of the corresponding orbitals with respect to the direction of the laser field and (ii) an increased ionization coming from the tail of the wave function in the direction of the ionization [59].

The energy ordering HOMO, HOMO-1, etc., refers to "global" properties of the orbitals averaged over space. The above arguments suggest that local properties, i.e., how much binding a certain part of the wave function feels, may play an important role. To illustrate this, Fig. 5(b) shows the average

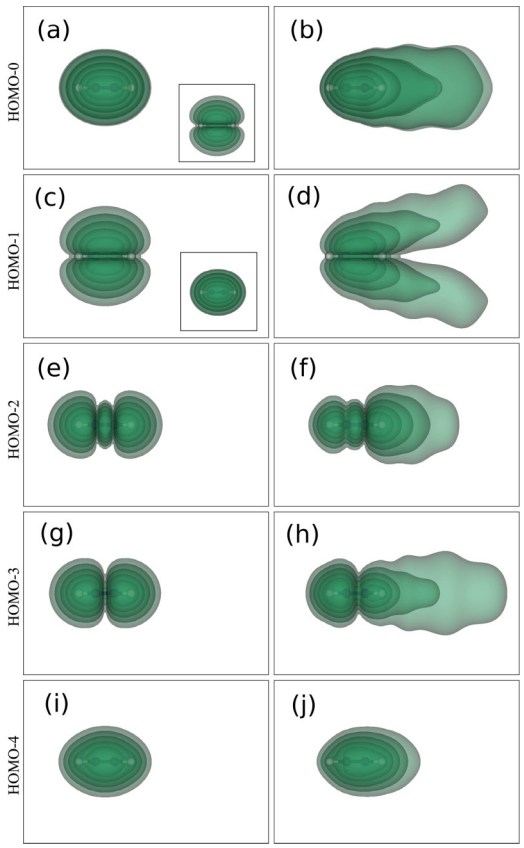

FIG. 4. (Color online) Time evolution of the Kohn-Sham orbitals in acetylene subjected to a 4.5-fs pulse with a peak intensity of 4×10^{14} W/cm^2 and field polarization parallel to the molecular axis. Here we show the absolute squares of the orbitals (left) at $t = 0$ fs and (right) at an instant when the laser field magnitude is near its peak at $t = 11.9$ fs. The insets show the HOMO and HOMO-1 rotated by 90° about the molecular axis. For an animated version, see the Supplemental Material [52].

density of the ground-state orbitals along the alignment axis of the molecule. Although the inner orbitals are more deeply bound, they have an extended weakly bound tail which strongly contributes to the ionization.

This picture is only valid for the ground-state: once the laser is turned on, ionization starts, and the potential and densities change. Nevertheless, this picture illustrates the origin of the larger contribution of the inner orbitals.

2. *Acetylene in a laser field polarized perpendicular to the molecular axis*

As the angle between the molecule and the laser field is increased to 22.5° and 45°, the kinetic energy of the protons and the total ionization decrease (see Table I). Eventually, the protons vibrate only in the perpendicular direction. With the molecular alignment axis perpendicular to the laser polarization, 4.5-fs pulses did not produce a Coulomb explosion in our simulations. Stronger pulses with a duration of 15 and 25 fs proved sufficient, however.

A one-dimensional projection of the Coulomb explosion in the perpendicular case is shown in Figs. 1(g)–1(j). The pulse width is 25 fs, and the intensity is 14×10^{14} W/cm^2. Unlike the parallel case, where the Coulomb explosion was due to the interplay of the laser force on the nuclei, the laser-induced oscillation of the electrons, and the ionization, here the fragmentation is the result of only bonds weakened by the ionization. The force exerted on the protons by the perpendicular laser field causes only a slight oscillation in the motion of the protons perpendicular to the molecular axis. However, the main component of the total force is due to the bond breaking, and the protons leave in the up and down directions symmetrically. Figure 2(d) shows the force on the protons. For a Coulomb explosion to occur a pulse stronger and longer than the one in the parallel case is required [see Figs. 2(a)–2(c)]. However, as seen in the parallel case, the model and Ehrenfest forces are very similar after the peak of the laser field.

We now turn to a more detailed analysis of the ionization dynamics using the full TDDFT model with Ehrenfest dynamics. Figures 3(d) and 3(e) show the total and orbital ionization dynamics. Due to the different symmetries, the ionization of the Kohn-Sham orbitals is quite different in the perpendicular case compared to the parallel one. Consider the short 4.5-fs pulse [Fig. 3(d)]. The ionization hierarchy of the orbitals from least to greatest is HOMO-4, HOMO-3, HOMO-2, HOMO, and HOMO-1. The two highest levels are no longer degenerate since the symmetry of the orbitals about the polarization axis has been broken. The tail of the HOMO-1 orbital in the direction of the laser polarization extends much farther than any of the other orbitals [see Fig. 5(b)]. Hence, the ionization overwhelmingly comes from the HOMO-1 orbital, and it loses more electrons than any of the orbitals in the parallel case.

Even at 14×10^{14} W/cm^2 the 4.5 fs pulse does not induce a Coulomb explosion. The two C-H bonds stretch symmetrically from 1.076 to 1.553 Å by the time that ionization completes.

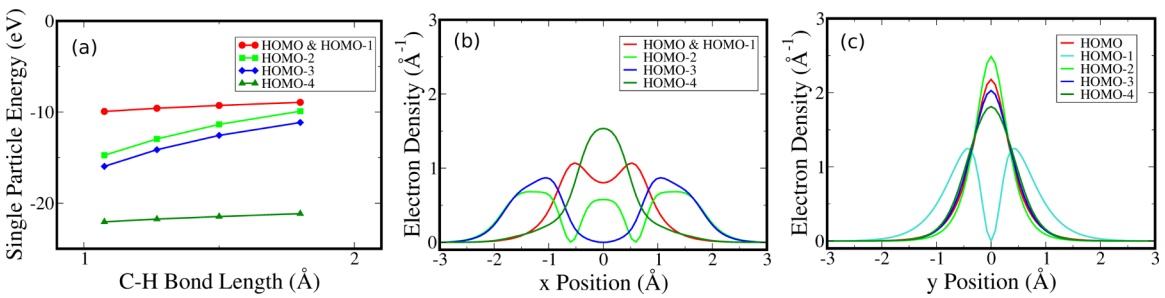

FIG. 5. (Color online) (a) The ground-state Kohn-Sham single-particle energies as a function of C-H bond length. (b) The average density of the ground-state Kohn-Sham orbitals along the alignment axis of the molecule (x axis). (c) The average density of the ground-state Kohn-Sham orbitals along an axis perpendicular to the alignment axis of the molecule (y axis). (b) and (c) refer to C_2H_2 in its equilibrium geometry.

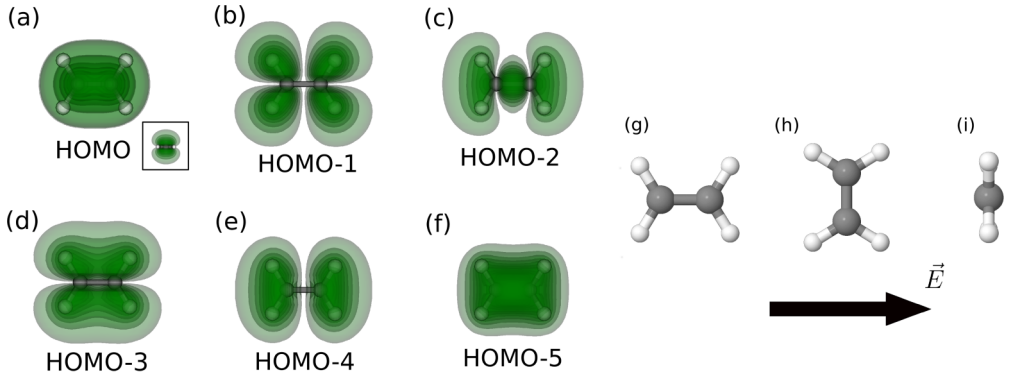

FIG. 6. (Color online) Ground-state Kohn-Sham orbitals of ethylene, C_2H_4. (a) The HOMO, with the inset showing a top-down view of the HOMO, (b) HOMO-1, (c) HOMO-2, (d) HOMO-3, (e) HOMO-4, and (f) HOMO-5. (g)–(i) The three molecular alignments relative to the electric field of the laser that are considered: (g) C-C parallel, (h) C-C bond perpendicular, and (i) all bonds perpendicular to the laser polarization.

This moderate increase in the bond length leads to a moderate enhanced ionization of 0.1 electron relative to the case where the ions are fixed in the ground state [see Fig. 3(d)]. Furthermore, the ionization from HOMO-2 and HOMO-3 remains small since there is no enhanced ionization.

Pulses with a duration of 15 and 25 fs and a peak intensity of 14×10^{14} W/cm^2 are now sufficient to cause a Coulomb explosion in the simulations. However, the kinetic energy of the emitted protons is about half that of the parallel case (see Table I). The bond stretching leads to an enhanced ionization effect not seen for the 4.5-fs pulses, and there is a substantial increase in the ionization from HOMO-2 [see Figs. 3(e) and 3(f)]. While HOMO-2 surpasses HOMO, HOMO-1 remains the dominant source of ionization. Unlike the parallel case, HOMO-3 plays very little role in the total ionization.

B. C_2H_4

The ionization and molecular dynamics of ethylene, C_2H_4, have been studied by varying the duration of the laser pulses (see Table I). The two laser pulses that we used exhibit an intensity and duration typical in experiments [31]. Three simple geometric alignments were considered [see Figs. 6(g)–6(i)].

We briefly describe the ions' dynamics observed in our simulations (see Table I). For the geometry with all bonds perpendicular to the laser polarization [Fig. 6(i)], the C-H bonds remain essentially unchanged, and the C-C bond stretches, but dissociation does not occur. For the geometry with only the C-C bond perpendicular to the laser polarization [Fig. 6(h)], the C-H bonds break slowly for the 9-fs pulse. At 17 fs the C-H bonds dissociate much more quickly due to the increased ionization. The C-C bond remains nearly unchanged for both pulses. For the geometry with the C-C bond parallel to the laser polarization [Fig. 6(g)], all of the C-H bonds fragment via a Coulomb explosion for both pulse durations. At the longer pulse duration of 17 fs the C-C bond also fragments.

We now turn to the orbital ionization dynamics. Figure 7 shows the occupation number of the time-dependent Kohn-Sham orbitals for the three geometries and the two laser pulses. When all bonds are aligned perpendicularly to the laser field [Fig. 6(i)], the HOMO nearly completely ionizes. HOMO-2 is the next most ionized, losing nearly 0.5 electron. The other orbitals stay unionized. Increasing the duration of the laser pulse has little effect on the orbital and total ionization.

We next consider the geometry where only the C-C bond is aligned perpendicular to the laser field [Fig. 6(h)]. The orbital ionization dynamics are dramatically different from the previous case. HOMO-1 is now the dominant source of ionization. At 9 fs HOMO, HOMO-2, and HOMO-3 each lose nearly 0.5 electron, while HOMO-4 and HOMO-5 are barely ionized. At 17 fs the C-H bonds stretch more quickly, causing a more pronounced enhanced ionization effect. Owing to both the direct effect of the increased pulse width and the enhanced ionization effect, the total ionization in the 17-fs pulse is increased by about 2 electrons. Furthermore, the inner orbitals, HOMO-2, HOMO-3, and HOMO-4, are

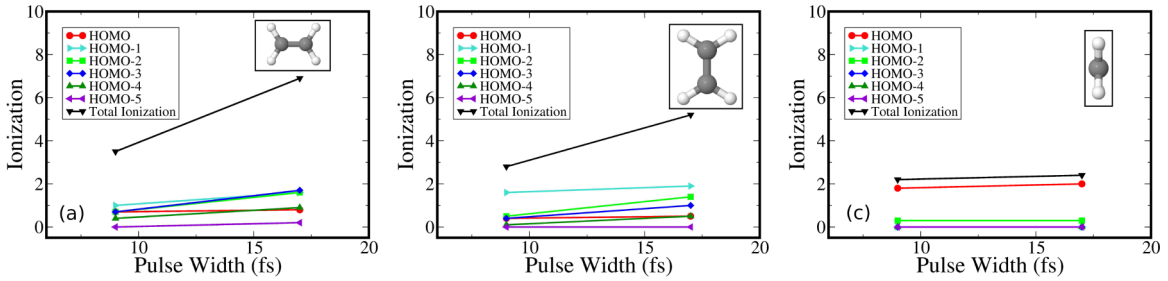

FIG. 7. (Color online) Total and orbital ionization as a function of laser pulse duration for three alignments of C_2H_4. The laser intensity is fixed at 8×10^{14} W/cm^2. C-C bond (a) parallel and (b) perpendicular to the laser polarization direction, with the C-H bonds neither parallel nor perpendicular to it. (c) All bonds are perpendicular to the laser polarization direction.

much more ionized, losing about 1.5, 1, and 0.5 electrons, respectively. The ionization dynamics from HOMO and HOMO-1 remain essentially unchanged by the increased pulse duration. HOMO-5 is unionized in either pulse.

Finally, we consider the geometry in Fig. 6(g). At a pulse duration of 9 fs HOMO-1 is again the most ionized orbital, losing nearly 1 electron. HOMO, HOMO-2, and HOMO-4 lose nearly 0.75 electron each. HOMO-4 loses somewhat less than 0.5 electron, and HOMO-5 stays unionized. For the 17-fs pulse, the total ionization is increased by both the direct effect of the longer pulse duration and a more prominent enhanced ionization effect. The enhanced ionization effect is increased since the bonds stretch at a much faster rate in the longer pulse. Hence, the molecule reaches a stretched configuration ($R \geqslant R_c$) earlier in the ionization process. Furthermore, the ionization of all orbitals except for HOMO has increased. HOMO-1, HOMO-2, and HOMO-3 are now nearly completely emptied. The ionization of HOMO-4 has overtaken the ionization from HOMO. The ionization from HOMO-5 increases to nearly 0.25 electron.

IV. SUMMARY

In summary, we have studied the ionization dynamics of acetylene, C_2H_2, and ethylene, C_2H_4, in strong laser pulses with various durations and peak intensities for different molecular alignments relative to the linear laser polarization direction using the TDDFT method. It is found that the molecular alignment has a dramatic effect on the total ionization. We have observed that bond stretching and bond breaking lead to an increase in the ionization efficiency, i.e., enhanced ionization, in qualitative agreement with previous theoretical investigations [38–40]. We have also calculated the ionization from individual Kohn-Sham orbitals. It was shown that the enhanced ionization mechanism primarily affects the inner valence orbitals. That is, the inner orbitals are more ionized when bond stretching occurs since they are more weakly bound in the stretched configurations. For some alignments and laser pulse parameters the ionization of the inner orbitals is greater than that of the highest occupied molecular orbital, owing to ionization from their extended weakly bound tails. Topics for future work include an investigation of larger polyatomic molecules and the effects of circular polarization. Future experiments planned for aligned molecules with short, strong laser pulses will be able to test the predictions of this paper and will stimulate further analysis.

ACKNOWLEDGMENTS

This work has been financed by the National Science Foundation (NSF) under Grants No. Phy 1314463 and No. IIA126117, the Vanderbilt University Discovery Grant, the Austrian Science Fund (FWF) under Grants No. P21463-N22, No. P25615-N27, and No. SFB-F49 NEXTlite, and a starting grant from the ERC (project CyFi).

[1] B. Manschwetus, T. Nubbemeyer, K. Gorling, G. Steinmeyer, U. Eichmann, H. Rottke, and W. Sandner, Phys. Rev. Lett. **102**, 113002 (2009).

[2] P. von den Hoff, I. Znakovskaya, M. F. Kling, and R. de Vivie-Riedle, Chem. Phys. **366**, 139 (2009).

[3] G. Sansone, F. Kelkensberg, J. F. Perez-Torres, F. Morales, M. F. Kling, W. Siu, O. Ghafur, P. Johnsson, M. Swoboda, E. Benedetti, F. Ferrari, F. Lepine, J. L. Sanz-Vicario, S. Zherebtsov, I. Znakovskaya, A. L'Huillier, M. Y. Ivanov, M. Nisoli, F. Martin, and M. J. J. Vrakking, Nature (London) **465**, 763 (2010).

[4] I. Bocharova, R. Karimi, E. F. Penka, J.-P. Brichta, P. Lassonde, X. Fu, J.-C. Kieffer, A. D. Bandrauk, I. Litvinyuk, J. Sanderson, and F. Légaré, Phys. Rev. Lett. **107**, 063201 (2011).

[5] X. Gong, Q. Song, Q. Ji, H. Pan, J. Ding, J. Wu, and H. Zeng, Phys. Rev. Lett. **112**, 243001 (2014).

[6] F. Krausz and M. Ivanov, Rev. Mod. Phys. **81**, 163 (2009).

[7] Y. Liu, X. Liu, Y. Deng, C. Wu, H. Jiang, and Q. Gong, Phys. Rev. Lett. **106**, 073004 (2011).

[8] X. Xie, K. Doblhoff-Dier, S. Roither, M. S. Schöffler, D. Kartashov, H. Xu, T. Rathje, G. G. Paulus, A. Baltuška, S. Gräfe, and M. Kitzler, Phys. Rev. Lett. **109**, 243001 (2012).

[9] X. Xie, K. Doblhoff-Dier, H. Xu, S. Roither, M. S. Schöffler, D. Kartashov, S. Erattupuzha, T. Rathje, G. G. Paulus, K. Yamanouchi, A. Baltuška, S. Gräfe, and M. Kitzler, Phys. Rev. Lett. **112**, 163003 (2014).

[10] X. Xie, S. Roither, M. Schöffler, E. Lötstedt, D. Kartashov, L. Zhang, G. G. Paulus, A. Iwasaki, A. Baltuška, K. Yamanouchi, and M. Kitzler, Phys. Rev. X **4**, 021005 (2014).

[11] V. Kumarappan, L. Holmegaard, C. Martiny, C. B. Madsen, T. K. Kjeldsen, S. S. Viftrup, L. B. Madsen, and H. Stapelfeldt, Phys. Rev. Lett. **100**, 093006 (2008).

[12] L. Holmegaard, J. H. Nielsen, I. Nevo, H. Stapelfeldt, F. Filsinger, J. Küpper, and G. Meijer, Phys. Rev. Lett. **102**, 023001 (2009).

[13] L. Holmegaard, J. L. Hansen, L. Kalhøj, S. L. Kragh, H. Stapelfeldt, F. Filsinger, J. Küpper, G. M. D. Dimitrovski, M. Abu-samha, C. P. J. Martiny, and L. B. Madsen, Nat. Phys. **6**, 428 (2010).

[14] C. Z. Bisgaard, O. J. Clarkin, G. Wu, A. M. D. Lee, O. Geßner, C. C. Hayden, and A. Stolow, Science **323**, 1464 (2009).

[15] M. Meckel, D. Comtois, D. Zeidler, A. Staudte, D. Pavičić, H. C. Bandulet, H. Pépin, J. C. Kieffer, R. Dörner, D. M. Villeneuve, and P. B. Corkum, Science **320**, 1478 (2008).

[16] S. Bubin, M. Atkinson, K. Varga, X. Xie, S. Roither, D. Kartashov, A. Baltuška, and M. Kitzler, Phys. Rev. A **86**, 043407 (2012).

[17] A. Talebpour, A. Bandrauk, J. Yang, and S. Chin, Chem. Phys. Lett. **313**, 789 (1999).

[18] B. K. McFarland, J. P. Farrell, P. H. Bucksbaum, and M. Gühr, Science **322**, 1232 (2008).

[19] H. Akagi, T. Otobe, A. Staudte, A. Shiner, F. Turner, R. Dörner, D. M. Villeneuve, and P. B. Corkum, Science **325**, 1364 (2009).

[20] P. Hoff, I. Znakovskaya, S. Zherebtsov, M. F. Kling, and R. Vivie-Riedle, Appl. Phys. B **98**, 659 (2009).

[21] Z. Wu, C. Wu, X. Liu, Y. Deng, Q. Gong, D. Song, and H. Su, J. Phys. Chem. A **114**, 6751 (2010).

[22] A. E. Boguslavskiy, J. Mikosch, A. Gijsbertsen, M. Spanner, S. Patchkovskii, N. Gador, M. J. J. Vrakking, and A. Stolow, Science **335**, 1336 (2012).
[23] J. Wu, L. P. H. Schmidt, M. Kunitski, M. Meckel, S. Voss, H. Sann, H. Kim, T. Jahnke, A. Czasch, and R. Dörner, Phys. Rev. Lett. **108**, 183001 (2012).
[24] C. Wu, H. Zhang, H. Yang, Q. Gong, D. Song, and H. Su, Phys. Rev. A **83**, 033410 (2011).
[25] J. Mikosch, A. E. Boguslavskiy, I. Wilkinson, M. Spanner, S. Patchkovskii, and A. Stolow, Phys. Rev. Lett. **110**, 023004 (2013).
[26] S. Weber, M. Oppermann, M. Ivanov, and J. Marangos, J. Mod. Opt. **60**, 1379 (2013).
[27] T. Seideman, M. Y. Ivanov, and P. B. Corkum, Phys. Rev. Lett. **75**, 2819 (1995).
[28] T. Zuo and A. D. Bandrauk, Phys. Rev. A **52**, R2511 (1995).
[29] D. M. Villeneuve, M. Y. Ivanov, and P. B. Corkum, Phys. Rev. A **54**, 736 (1996).
[30] S. Roither, X. Xie, D. Kartashov, L. Zhang, M. Schöffler, H. Xu, A. Iwasaki, T. Okino, K. Yamanouchi, A. Baltuska, and M. Kitzler, Phys. Rev. Lett. **106**, 163001 (2011).
[31] X. Xie, S. Roither, M. Schöffler, H. Xu, S. Bubin, E. Lötstedt, S. Erattuphuza, A. Iwasaki, D. Kartashov, K. Varga, G. G. Paulus, A. Baltuška, K. Yamanouchi, and M. Kitzler, Phys. Rev. A **89**, 023429 (2014).
[32] E. Runge and E. K. U. Gross, Phys. Rev. Lett. **52**, 997 (1984).
[33] P. Ehrenfest, Z. Phys. **45**, 455 (1927).
[34] M. V. Ammosov, N. B. Delone, and V. P. Krainov, Sov. Phys. JETP **64**, 1191 (1986).
[35] X. M. Tong, Z. X. Zhao, and C. D. Lin, Phys. Rev. A **66**, 033402 (2002).
[36] K. Codling, L. J. Frasinski, and P. A. Hatherly, J. Phys. B **22**, L321 (1989).
[37] D. Dimitrovski, C. P. J. Martiny, and L. B. Madsen, Phys. Rev. A **82**, 053404 (2010).
[38] E. Lötstedt, T. Kato, and K. Yamanouchi, Phys. Rev. A **85**, 041402 (2012).
[39] E. Lötstedt, T. Kato, and K. Yamanouchi, Phys. Rev. A **86**, 023401 (2012).
[40] E. Lötstedt, T. Kato, and K. Yamanouchi, J. Chem. Phys. **138**, 104304 (2013).
[41] E. Livshits and R. Baer, J. Phys. Chem. A **110**, 8443 (2006).
[42] M. Isla and J. A. Alonso, J. Phys. Chem. C **111**, 17765 (2007).
[43] M.-P. Gaigeot, P. Lopez-Tarifa, F. Martin, M. Alcami, R. Vuilleumier, I. Tavernelli, M.-A. H. du Penhoat, and M.-F. Politis, Mutat. Res. Rev. Mutat. Res. **704**, 45 (2010).
[44] A. Debnarova, S. Techert, and S. Schmatz, Phys. Chem. Chem. Phys. **14**, 9606 (2012).
[45] Y. Kawashita, T. Nakatsukasa, and K. Yabana, J. Phys.: Condens. Matter **21**, 064222 (2009).
[46] J. Haruyama, C. Hu, and K. Watanabe, Phys. Rev. A **85**, 062511 (2012).
[47] N. Troullier and J. L. Martins, Phys. Rev. B **43**, 1993 (1991).
[48] J. P. Perdew and A. Zunger, Phys. Rev. B **23**, 5048 (1981).
[49] A. Castro, M. A. L. Marques, and A. Rubio, J. Chem. Phys. **121**, 3425 (2004).
[50] D. E. Manolopoulos, J. Chem. Phys. **117**, 9552 (2002).
[51] *NIST Chemistry WebBook, NIST Standard Reference Database Number 69*, edited by P. J. Linstrom and W. G. Mallard (NIST, Gaithersburg, MD, 2001).
[52] See Supplemental Material at http://link.aps.org/supplemental/10.1103/PhysRevA.91.023422 for an animation of the time evolution of the Kohn-Sham orbitals.
[53] I. V. Litvinyuk, F. Légaré, P. W. Dooley, D. M. Villeneuve, P. B. Corkum, J. Zanghellini, A. Pegarkov, C. Fabian, and T. Brabec, Phys. Rev. Lett. **94**, 033003 (2005).
[54] W. A. Bryan, S. L. Stebbings, J. McKenna, E. M. L. English, M. Suresh, J. Wood, B. Srigengan, I. C. E. Turcu, J. M. Smith, E. J. Divall, C. J. Hooker, A. J. Langley, J. L. Collier, I. D. Williams, and W. R. Newell, Nat. Phys. **2**, 379 (2006).
[55] T. Kanai, S. Minemoto, and H. Sakai, Nature (London) **435**, 470 (2005).
[56] W. Li, X. Zhou, R. Lock, S. Patchkovskii, A. Stolow, H. C. Kapteyn, and M. M. Murnane, Science **322**, 1207 (2008).
[57] X. Zhou, R. Lock, W. Li, N. Wagner, M. M. Murnane, and H. C. Kapteyn, Phys. Rev. Lett. **100**, 073902 (2008).
[58] W. Boutu, S. Haessler, H. Merdji, P. Breger, G. Waters, M. Stankiewicz, L. J. Frasinski, R. Taieb, J. Caillat, A. Maquet, P. Monchicourt, B. Carre, and P. Salieres, Nat. Phys. **4**, 545 (2008).
[59] O. Smirnova, Y. Mairesse, S. Patchkovskii, N. Dudovich, D. Villeneuve, P. Corkum, and M. Y. Ivanov, Nature (London) **460**, 972 (2009).